Journal of Environmental Management 339 (2023) 117938

Contents lists available at ScienceDirect

Journal of Environmental Management

journal homepage: www.elsevier.com/locate/jenvman

Research article

Designing low-carbon cement-free binders for stabilization/solidification of MSWI fly ash

Chen Sun [a], Weizhe Ge [a], Yuying Zhang [b,a], Lei Wang [a,*], Yan Xia [a,c], Xiaoqing Lin [a], Qunxing Huang [a], Shengyong Lu [a], Daniel C.W. Tsang [b,a], Jianhua Yan [a]

[a] State Key Laboratory of Clean Energy Utilization, Zhejiang University, Hangzhou, 310027, China
[b] Department of Civil and Environmental Engineering, The Hong Kong Polytechnic University, Hung Hom, Kowloon, Hong Kong, China
[c] School of Civil Engineering, Harbin Institute of Technology, Harbin, 150090, China

ARTICLE INFO

Keywords:
Waste incineration fly ash
Hazardous waste treatment
Low-carbon stabilization/solidification
PTEs leachability
Sustainable waste management

ABSTRACT

Low-carbon and high-efficiency binder is desirable for sustainable treatment of municipal solid waste incineration fly ash (MSWI FA). In this study, CaO or MgO was used to activate ground granulated blast furnace slag (GGBS) to form calcium silicate hydrate and magnesium silica hydrate gel for stabilization/solidification of hazardous MSWI FA. Experimental results showed that potential toxic elements (PTEs), such as Pb and Zn, significantly inhibited the formation of reaction products in CaO-GGBS system due to the complexation between $Ca(OH)_2$ and PTEs, whereas PTEs only had insignificant inhibition on transformation from MgO to $Mg(OH)_2$ in MgO-GGBS system, resulting in lower leachabilities of PTEs and higher mechanical strengths. Stabilization/solidification experiments demonstrated that MSWI FA (70 wt%) could be recycled by MgO-GGBS binder (30 wt%) into blocks with desirable 28-day compressive strengths (3.9 MPa) and PTEs immobilization efficiencies (99.8% for Zn and 99.7% for Pb). This work provides mechanistic insights on the immobilization mechanisms of PTEs in CaO/MgO-GGBS systems and suggests a promising MgO-GGBS binder for low-carbon treatment of MSWI FA.

1. Introduction

Incineration has been the principal treatment technology for dealing with mass volumes of municipal solid wastes in recent years, owing to the advantages of both energy generation and volume reduction. However, the incineration process inevitably generates municipal solid waste incineration fly ash (MSWI FA), which is equivalent to 3–5 wt% of waste combusted in the moving grate furnace and approximately 12 wt% of waste combusted in the circulating fluidized bed furnace (Funari et al., 2015). In China, the annual generation of MSWI FA reaches more than 7 million tonnes (NBSC, 2020). Considering the high contents of potentially toxic elements (PTEs) (Fan et al., 2022) and persistent organic pollutants (e.g., dioxin), MSWI FA is globally categorized as a hazardous waste (Ma et al., 2019). The dioxin emission could be significantly reduced owing to the state-of-the-art incineration and air pollution control technology, whereas PTEs treatment is still the major challenge for the safe disposal of MSWI FA in compliance with the national standard (GB, 2017).

Stabilization/solidification (S/S) is a mature technology for the treatment of PTEs-rich hazardous waste (Zhou et al., 2022). After the S/S treatment, PTEs can be efficiently immobilized and the S/S products may be recycled as sustainable construction materials (Xia et al., 2023a, 2023b). Ordinary Portland cement (OPC) is the most widely adoptable binder for the S/S treatment (Trauchessec et al., 2015). However, the high contents of Zn (3000–7000 mg/kg) and Pb (1000–3000 mg/kg) in MSWI FA (Lan et al., 2022; Quina et al., 2008) would greatly inhibit the hydration process of OPC, resulting in unsatisfactory immobilization efficiency and poor strength development. For example, 0.1 wt% ZnO addition would delay the setting time of the OPC system by 3.5–4 times, and 0.7 wt% ZnO addition would thoroughly terminate cement hydration (Wang et al., 2020). This was because the formation of $Ca(Zn(OH)_3)_2{\cdot}2H_2O$ deteriorated the nucleation and growth of calcium silicate hydrate (C–S–H) (Garg and White, 2017; Liu et al., 2019). Similarly, in a Pb-incorporated cement system, the formation of Pb-containing oxides and hydroxides (PbO, $Pb(OH)_2$, or $PbOPb(OH)_2$) would cover the surface of clinker particles and interfere with the initial hydration process (Wang et al., 2018; Ren et al., 2023). Moreover, the over-high pH value of OPC system (>13) is unsuitable for the immobilization of amphoteric metals (Zn, Pb, etc.), which would be stabilized at a pH of 10 (Paria and

* Corresponding author.
E-mail address: wanglei.leo@zju.edu.cn (L. Wang).

https://doi.org/10.1016/j.jenvman.2023.117938
Received 27 January 2023; Received in revised form 1 April 2023; Accepted 11 April 2023
Available online 18 April 2023

List of abbreviations

Abbreviation and description	
MSWI FA	municipal solid waste incineration fly ash
GGBS	ground granulated blast furnace slag
C–S–H	calcium silicate hydrate
M-S-H	magnesium silica hydrate
TCLP	toxicity characteristic leaching procedure
PTEs	potential toxic elements
OPC	ordinary Portland cement
MOSC	magnesium oxysulfate cement
MPC	magnesium phosphate cement
S/S	stabilization/solidification

Yuet, 2006; Wang and Wang, 2022).

In comparison with Ca-based cementitious materials, Mg-based cement provided a superior S/S performance on Zn- and Pb-enriched wastes owing to the favorable compatibility and moderate alkaline environment (pH 9–12) (Walling and Provis, 2016; Li et al., 2019). Our previous studies found that the incorporation of 10 wt% ZnO in the magnesium oxysulfate cement (MOSC) system only delayed the setting time by 14% (Guo et al., 2021). In addition, the MOSC system also exhibited a satisfactory immobilization efficiency for Pb and As (Wang et al., 2022), while magnesium phosphate cement (MPC) demonstrated high compatibility with Zn-rich sludge (Zhang et al., 2022). However, the high cost of raw materials may restrict the large-scale application of MOSC and MPC binders. Among the magnesium cement family, magnesium silicate hydrate (M-S-H) cement is a cost-effective and low-carbon binder from low-cost industrial by-products. The Si-rich inorganic wastes could be activated by reactive MgO to generate M-S-H gel, which may offer superior immobilization efficiency, high compressive strength (20–70 MPa), and good durability (Martini et al., 2017). Granulated ground blast furnace slag (GGBS) is a Si and Al-rich industrial by-product, which could be used as a precursor to generate M-S-H gel (Haha et al., 2011, 2012; Zhang et al., 2020). The energy consumption (1300 MJ/tonne) and carbon emission (0.07 tonne CO_2 per tonne) of GGBS are much lower than that of OPC (5000 MJ/tonne and 0.8 tonne CO_2 per tonne) (Abdalqader et al., 2016). Therefore, the MgO-GGBS system may serve as a low-carbon binder for S/S of PTEs in hazardous wastes, yet a deep understanding of the inhibition effects of PTEs on the reaction of GGBS-based binders is still lacking. The

Table 1
Main compositions of the ingredients based on XRF analysis.

	CaO	MgO	SiO_2	Al_2O_3	Cl	SO_3	Na_2O	K_2O	Fe_2O_3
MSWI fly ash	38.49	1.08	6.24	1.62	22.03	11.13	10.56	6.62	2.23
GGBS	40.63	8.17	31.97	14.06	0.02	2.50	0.30	0.48	1.86
MgO	1.74	93.62	3.49	0.33	0.04	0.14	0.00	0.00	0.64

Table 2
Mixture design for CaO- and MgO-GGBS pastes and MSWI FA S/S blocks (wt%).

	CaO	MgO	GGBS	$Pb(NO_3)_2$	$Zn(NO_3)_26H_2O$[b]	MSWI FA	W/B (water/binder)
C1G9	10	/	90	/	/	/	0.35
C2G8	20	/	80	/	/	/	0.35
M1G9	/	10	90	/	/	/	0.37
M2G8	/	20	80	/	/	/	0.37
C1G9-Pb[a]	/	9	81	10	/	/	0.42
C1G9-Zn	/	9	81	/	15.7	/	0.36
M2G8-Pb	/	18	72	10	/	/	0.43
M2G8-Zn	/	18	72	/	15.7	/	0.38
C1G9F5[c]	5	/	45	/	/	50	0.40
C1G9F7	3	/	27	/	/	70	0.42
C1G9F9	1	/	9	/	/	90	0.44
M2G8F5	/	10	40	/	/	50	0.41
M2G8F7	/	6	24	/	/	70	0.43
M2G8F9	/	2	8	/	/	90	0.44

[a] Water-to-metal salt ratio = 1 (same for C1G9-Zn, M2G8-Pb and M2G8-Zn).
[b] Crystal water mass is deducted in the required water content.
[c] Water-to-MSWI FA ratio = 0.45 (same for other following five recipes).

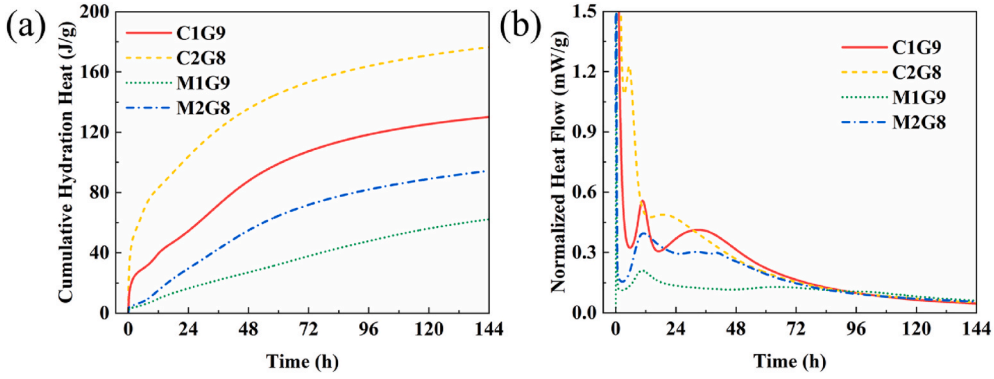

Fig. 1. Isothermal calorimetry of CaO and MgO activated GGBS pastes.

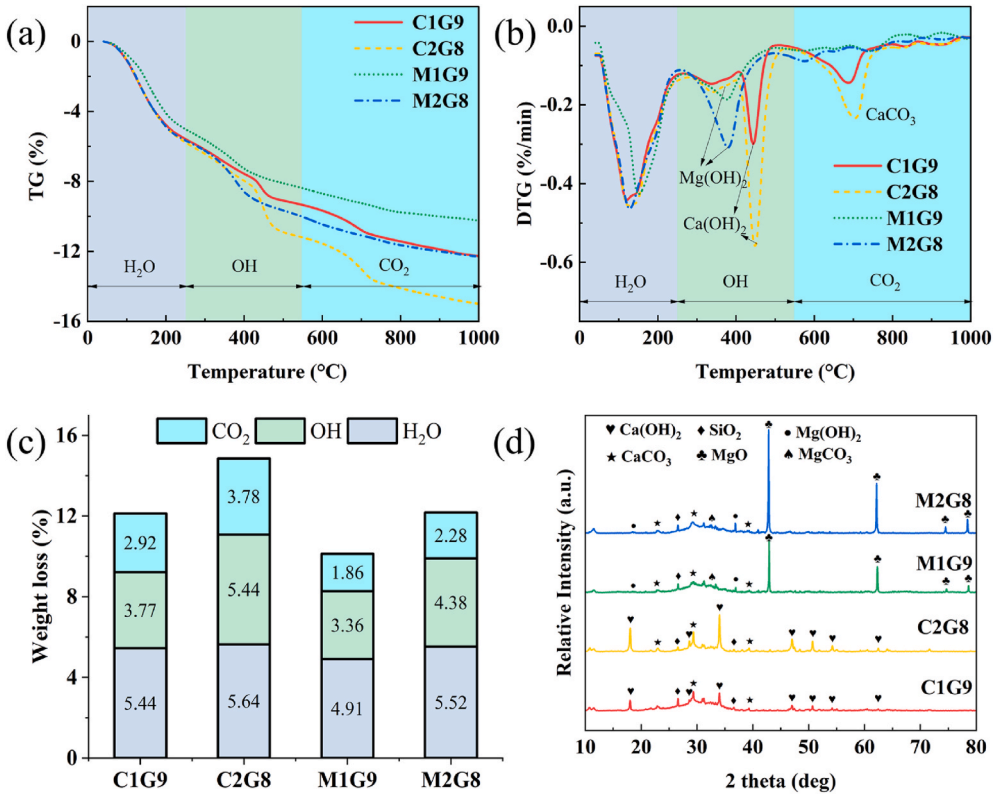

Fig. 2. TGA and XRD of 28-day CaO and MgO activated GGBS pastes.

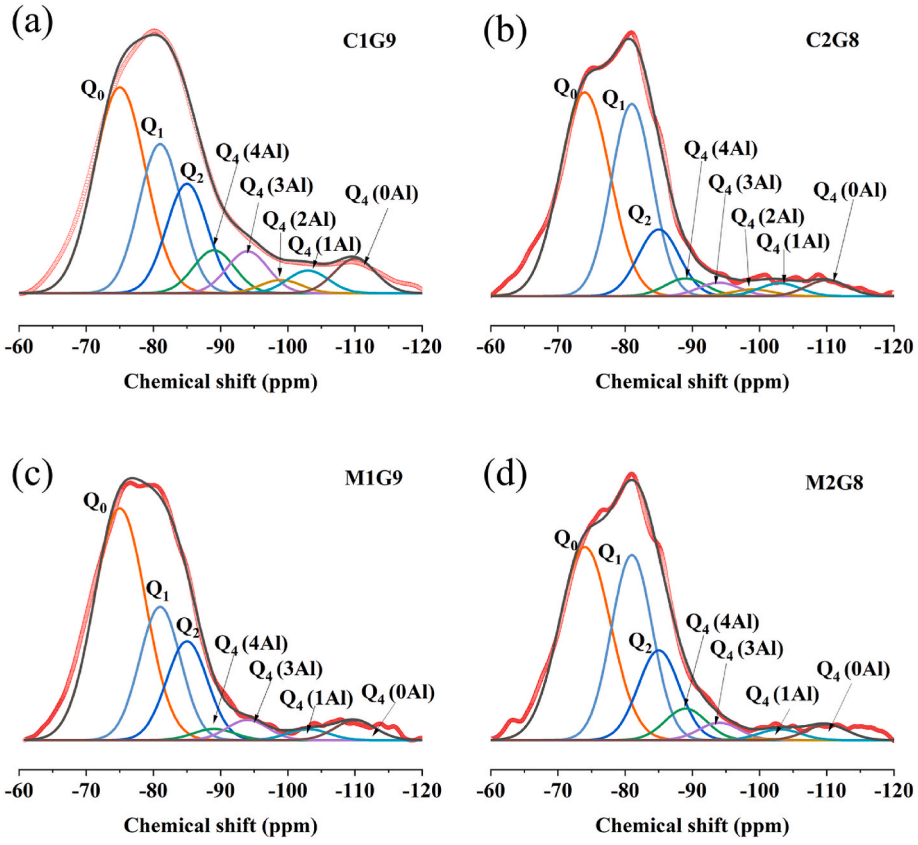

Fig. 3. ^{29}Si MAS NMR spectra and the associated deconvolutions for various pastes.

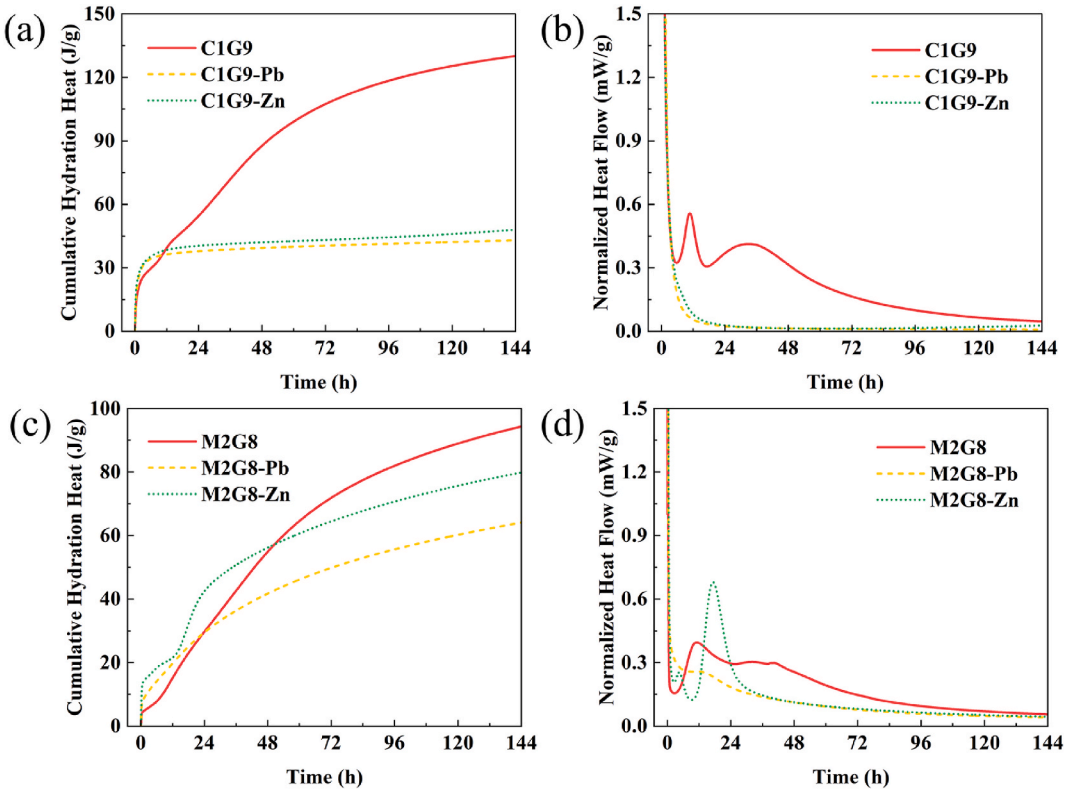

Fig. 4. Isothermal calorimetry of Pb- or Zn-incorporated pastes.

immobilization capacities and mechanisms of PTEs in CaO-/MgO-GGBS systems should also be clarified. The feasibility of such low-carbon binder systems in S/S of MSWI FA requires comprehensive evaluation.

In this study, CaO-GGBS and MgO-GGBS systems are designed for the S/S of MSWI FA. The inhibition effects and the immobilization mechanisms of PTEs (i.e., Pb and Zn) in CaO-/MgO-GGBS binders are elaborated with the aid of comprehensive characterization techniques. The practical performance of CaO and MgO activated GGBS binders for S/S of MSWI FA is thoroughly evaluated. This study would provide insights into the interactions between PTEs and Ca- or Mg-based binders, and offer a low-carbon treatment strategy for MSWI FA.

2. Materials and methods

2.1. Materials

MSWI FA was collected in a moving grate furnace of a waste incineration plant in Jiangyin, Jiangsu Province, China. All the concentrations of polychlorinated dibenzo-p-dioxins and dibenzofurans (PCDD/Fs) were below the national limits (GB 18485, 2014). The GGBS was from an iron and steel company in Zhejiang Province, China. Detailed information on MSWI FA and GGBS is presented in **Text S1** (Supplementary Information). In addition, the light-burned MgO with a purity of 93.6% (shown in Table 1) and CaO with a purity of 99.9% were used to activate GGBS (Liew et al., 2019; Yek et al., 2020). The Zn $(NO_3)_2{\cdot}6H_2O$ (>98%) from Aladdin reagents, $Pb(NO_3)_2$ (>99%, AR), and acetic acid (GR >99.8%) from Sinopharm Chemical Reagent Co., Ltd were also used in this study.

2.2. Sample preparation

Recipes for different pastes and S/S mixtures are listed in Table 2. For MSWI FA-derived pastes, the incorporation ratio varied from 50 to 90 wt %. During the S/S process, pre-weighed dry powders were first dry-mixed for 1 min before adding water. Noted that in the metal-incorporated mixtures, metal salts are pre-dissolved in the water before mixing. The mixture of powder and water was then mixed for 3 min to form a homogeneous paste. Then, the well-mixed mixtures were poured into cubic molds ($2 \times 2 \times 2$ cm^3), and were demolded after one day. The demolded samples were stored in a curing chamber at 20 °C with 95% relative humidity for additional 27 days (28 days in total). All the samples were prepared in triplicates for compressive strength tests.

2.3. Tests and characterization

The compressive strengths of S/S samples after 28-day curing were tested by using a mechanical testing machine (CYW-4050, Chengyu, China) at a loading rate of 0.3 MPa s^{-1} according to an international standard (BS EN 12390-3, 2009). The leachabilities of PTEs from raw MSWI FA and 28-day cured samples are performed according to the TCLP procedure (US EPA 1311, 1992). Each sample was conducted two times, error bars were given in related figures and tables. The concentrations of PTEs in the leachate were detected using inductively coupled plasma-atomic emission spectrometry (ICP-AES, iCAP 6300, thermos, USA). Quality assurance and quality control (QA/QC) for each element analysis were performed by using the standard calibration curve (R^2 > 0.999). All the 28-d cured samples were first crushed into small particles (<2.36 mm) and immersed in isopropanol to terminate the hydration process. The samples were subsequently crushed into powders with

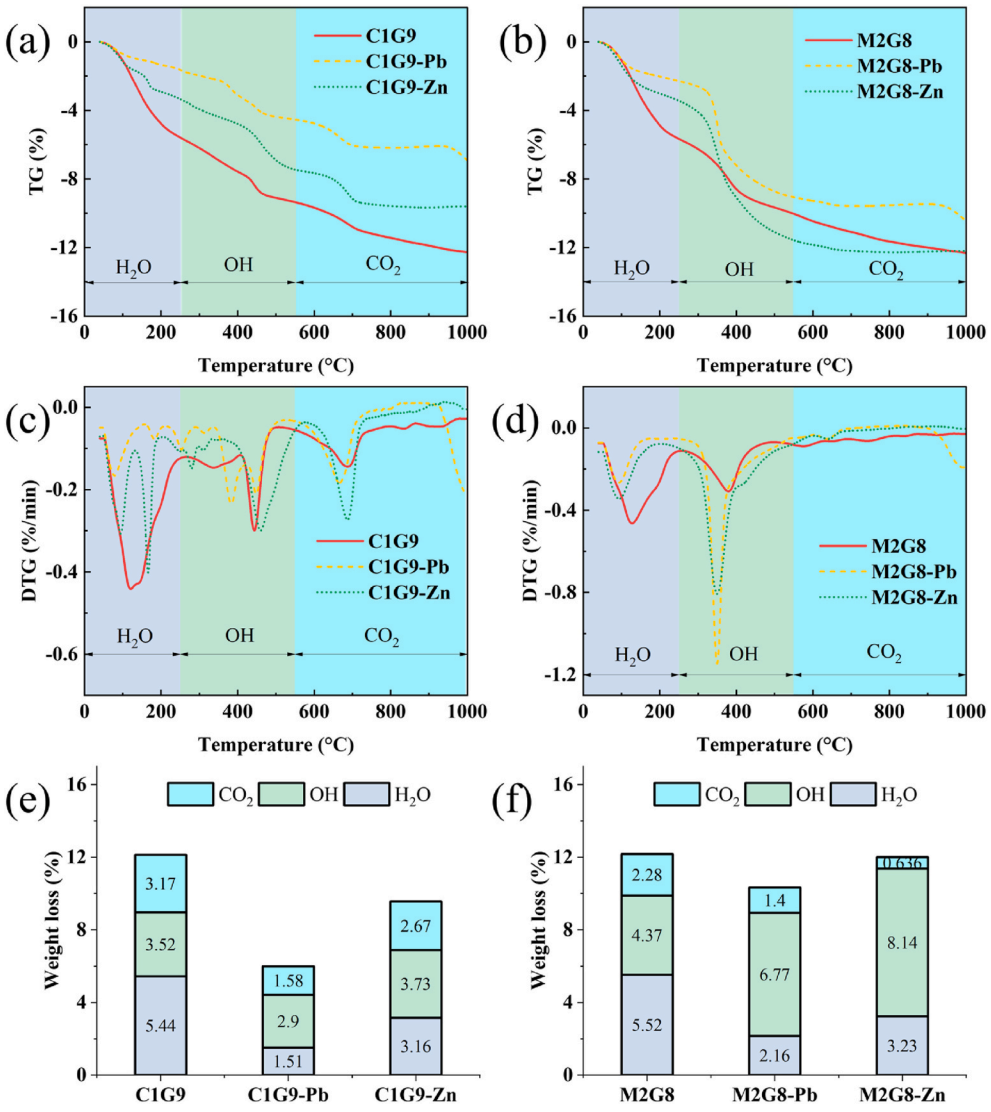

Fig. 5. TGA of 28-day Pb or Zn-incorporated pastes.

particle sizes less than 0.1 mm before the thermogravimetric analysis (TGA), the X-ray diffraction (XRD), and nuclear magnetic resonance (NMR) tests, related details of the above-mentioned tests are shown in **Text S1**.

3. Results and discussion

3.1. Comparison of CaO- and MgO-activated GGBS systems

Heat evolution curves show that the MgO-GGBS systems had a milder reaction than the CaO-GGBS systems at the early stage. As shown in Fig. 1a, the CaO-activated GGBS system released nearly twice as much heat as the MgO-activated GGBS system at the same dosage. This could be ascribed to the comparatively fast dissolution and high alkalinity of CaO. The dosages of activators affect heat release. With the blending ratio increasing from 10% to 20%, the cumulative hydration heat increased from 125 to 179 J/g in the CaO-GGBS system and 61–94 J/g in the MgO-GGBS system. Fig. 1b exhibits that two reaction peaks emerge in both CaO and MgO-activated systems during the 144-h reaction. The first reaction peak could be ascribed to the hydration of silicates, while the second could be attributed to the aluminate hydration (Whittaker et al., 2014). The time to reach the first reaction peak (TTRP) of C2G8 (5.3 h) was half of M2G8 (10.8 h), indicating a vigorous reaction process of the CaO-GGBS system at the early stage. The heat flow of the MgO-GGBS system bypassed the value of the CaO-GGBS system after 96 h, reflecting a mild and continued reaction of the MgO-GGBS system. It is noted that over vigorous reaction would result in an insufficient reaction at the later stage and even serious cracking, which is unfavorable for the continued reaction and strength development of cementitious materials (Li et al., 2020). Therefore, C1G9 and M2G8 mixtures with mild reaction processes were selected as the binders for subsequent S/S experiments.

The TGA results illustrate the hydration degree of various CaO- and MgO-activated GGBS systems. The TG curves in Fig. 2a&b could be divided into three temperature zones (Chen et al., 2022): (i) the weight loss between 60 °C and 250 °C could be attributed to the evolution of adsorbed or bound water (Jin and Al-Tabbaa, 2013; Rheinheimer et al., 2017); (ii) the weight loss from 250 to 550 °C could be ascribed to the decomposition of different hydroxides, e.g., $Ca(OH)_2$ (peaked at 450–550 °C), $Mg(OH)_2$ (peaked at 350–400 °C), etc. (Wang and Fan, 2020); (ii) the weight loss peak over 550 °C is due to the decomposition of carbonates (Hay and Celik, 2020). The weight losses in each zone are summarized in Fig. 2c. The C1G9 (5.44%) and C2G8 (5.64%) contained comparable bound water contents, implying the similar content of C–S–H gel in each sample. The abundant $Ca(OH)_2$ formation in the C2G8 sample was evidenced by the XRD results (Fig. 2d). In MgO-activated

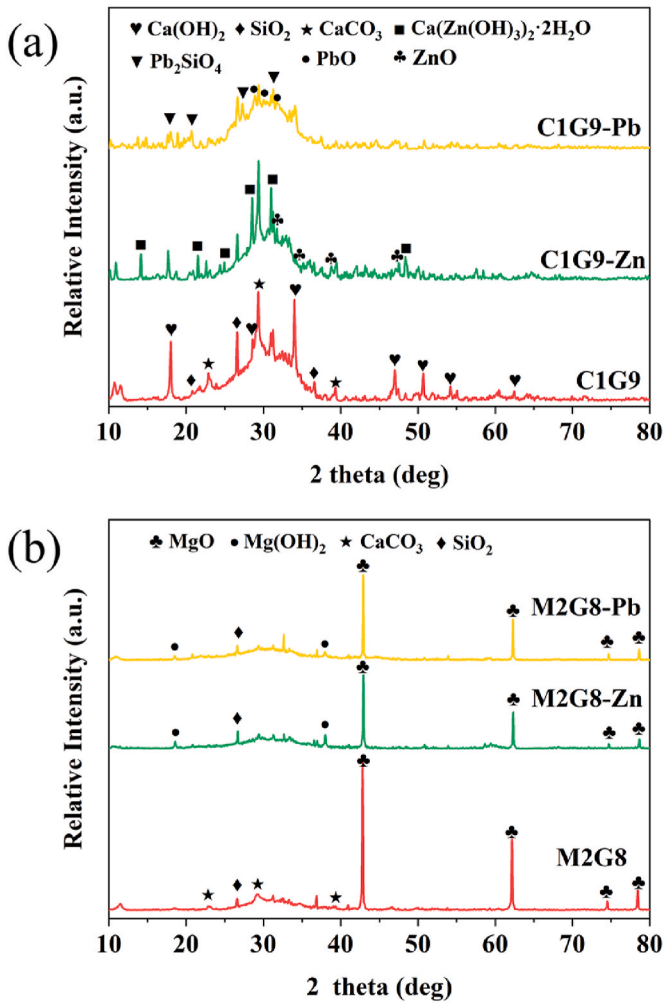

Fig. 6. XRD patterns of 28-day Pb- or Zn-incorporated pastes.

system, as the MgO dosage increased, the bound water content increased from 4.91 to 5.52%, illustrating that a greater content of M-S-H gel formation was induced by a higher dosage of MgO. These results above illustrated that 10% CaO was sufficient to generate C–S–H gel, while 20% MgO addition was necessary to promote the formation of M-S-H gel. The carbonate content of MgO-GGBS system was much lower than that of CaO-GGBS system, which could be attributed to the limited Mg $(OH)_2$ content for carbonation.

The XRD patterns of the pastes (Fig. 2d) illustrated the various hydration products in CaO- and MgO-activated GGBS systems. Broad peaks centered at approximately 30° could be the signal of the C–S–H or M-S-H gel (Jin and Al-Tabbaa, 2013). The $Ca(OH)_2$ peaks appeared in C1G9 and C2G8 samples, which could be the intermediate from CaO to C–S–H gel. As the CaO dosage increased, the peak intensity of $Ca(OH)_2$ increased, indicating that more $Ca(OH)_2$ was generated in the C2G8 sample. In contrast, the intensities of $Mg(OH)_2$ in M1G9 and M2G8 pastes were very weak, possibly inferring adequate reaction between Mg $(OH)_2$ and reactive silica in GGBS to form M-S-H gel (Jin and Al-Tabbaa, 2013). This phenomenon indicated that the generation rate of $Mg(OH)_2$ was slower than its consumption rate. The MgO residue in M1G9 and M2G8 samples also implied the slow hydration rates of selected MgO.

The ^{29}Si MAS NMR spectra exhibit that 10% CaO effectively activated the GGBS reaction, whereas 20% MgO was required for deep activation of GGBS. All the spectra are deconvolved into eight peaks at the chemical shift of −75 ppm (Q_0), −80 ppm (Q_1), −85 ppm (Q_2), −89 ppm (Q_4 (4Al)), −94 ppm (Q_4 (3Al)), −99 ppm (Q_4 (2Al)), −103 ppm (Q_4 (1Al)), and −110 ppm (Q_4 (0Al)), respectively (Walkley and Provis, 2019). The ^{29}Si MAS NMR spectra and the associated deconvolution curves are shown in Fig. 3, and the derived relative integral area ratios are listed in Table S2. Compared to the Q_0 ratio (49.0%) in the raw GGBS, the Q_0 ratio in C1G9 decreased by 22%, whereas the Q_0 ratio in M1G9 nearly unchanged. This confirmed that 10% CaO in C1G9 effectively activated the reaction of GGBS, however, 10% MgO in M1G9 was not sufficient for activation. As the dosage of MgO increased, the Q_0 ratio decreased from 49.6% (M1G9) to 40.7% (M2G8), while the Q_1 ratio increased from 22.8% (M1G9) to 31.2% (M1G9), corroborating that 20% dosage of MgO could effectively activate the reaction of GGBS.

The CaO-activated GGBS systems had higher compressive strengths than that of MgO-activated GGBS systems. As shown in Fig. S3, C1G9 and C2G8 could reach approximately 18 MPa after 7-day curing; M1G9 and M2G8 achieved only 10.3 and 15.6 MPa, respectively. After 28-day curing, the strength of C1G9 and C2G8 elevated to 30.1 MPa and 34.9 MPa, respectively, which was also higher than those of M1G9 (24.4 MPa) and M2G8 (27.3 MPa). These results illustrated that CaO-based GGBS binder could offer higher strength than MgO-based GGBS binder (Chen and Ye, 2022), and the 10% CaO in C1G9 was sufficient for activating GGBS whereas 20% MgO in M2G8 was required for effective activation. Therefore, C1G9 and M2G8 binders were selected for subsequent S/S of PTEs and MSWI FA.

3.2. Inhibition effects of Pb and Zn on CaO-/MgO-GGBS reaction

The incorporation of Pb and Zn significantly suppressed the heat release of the CaO-GGBS system, while selected PTEs slightly inhibited the reaction of the MgO-GGBS system. From Fig. 4a, Pb or Zn addition nearly halted the reaction process of the C1G9-based binder; the cumulative heat release over 144 h decreased by 64%. No reaction peaks appeared in the heat flow curves of C1G9-Pb or Zn (Fig. 4b). By comparison, the incorporation of Zn and Pb only decreased the 144-h cumulative heat evolution of M2G8-system by 16% and 32%, respectively (Fig. 4c). The TTRPs of M2G8-Pb and M2G8-Zn in Fig. 4d were prolonged from 10.8 h to 13.0 and 17.3 h, which were still acceptable. (Guo et al., 2021; Wang et al., 2022).

The TGA results illustrated the PTEs significantly inhibited the hydration process from CaO to $Ca(OH)_2$ in the CaO-GGBS system, whereas PTEs did not hinder the conversion from MgO to $Mg(OH)_2$, but only influenced the transformation from $Mg(OH)_2$ to M-S-H gel. As shown in Fig. 5e, the bound water contents of C1G9-Pb and C1G9-Zn were only 1.51% and 3.16%, i.e., much less than that in C1G9 (5.58%), suggesting that the incorporation of Pb or Zn significantly inhibited the formation of C–S–H gel. This trend also agreed with the reduction of heat release in the ICC curves. Compared to the hydroxide content (3.52%) in C1G9, the content in C1G9-Pb (2.9%) was relatively low, while the value in C1G9-Zn was comparable. The above results revealed that Pb or Zn addition inhibited the conversion from CaO to $Ca(OH)_2$. As for M2G8-based systems shown in Fig. 5f, the bound water contents significantly decreased from 5.52% to 2.16% or 3.23% after Pb or Zn incorporation, respectively. However, the hydroxide contents in M2G8-Pb (6.77%) and M2G8-Zn (8.14%) were higher than that in M2G8 (4.37%). This phenomenon indicated that PTEs only suppressed the transformation from $Mg(OH)_2$ to M-S-H gel, but showed less inhibition effect on the conversion from MgO to $Mg(OH)_2$. Therefore, compared to the CaO-GGBS system, the MgO-GGBS system showed high compatibility with PTEs.

3.3. Immobilization mechanisms of Pb and Zn by CaO-/MgO-GGBS binders

The XRD patterns clearly illustrate the Zn and Pb in CaO-GGBS systems could form $Ca(Zn(OH)_3)_2{\cdot}2H_2O$ and $2PbO{\cdot}SiO_2$, respectively, whereas Zn and Pb in MgO-GGBS systems were immobilized by forming through encapsulation in abundant hydration products. As shown in Fig. 6a, the incorporation of Zn and Pb significantly decreased the peak intensity of $Ca(OH)_2$ in the C1G9-based system, which was in line with

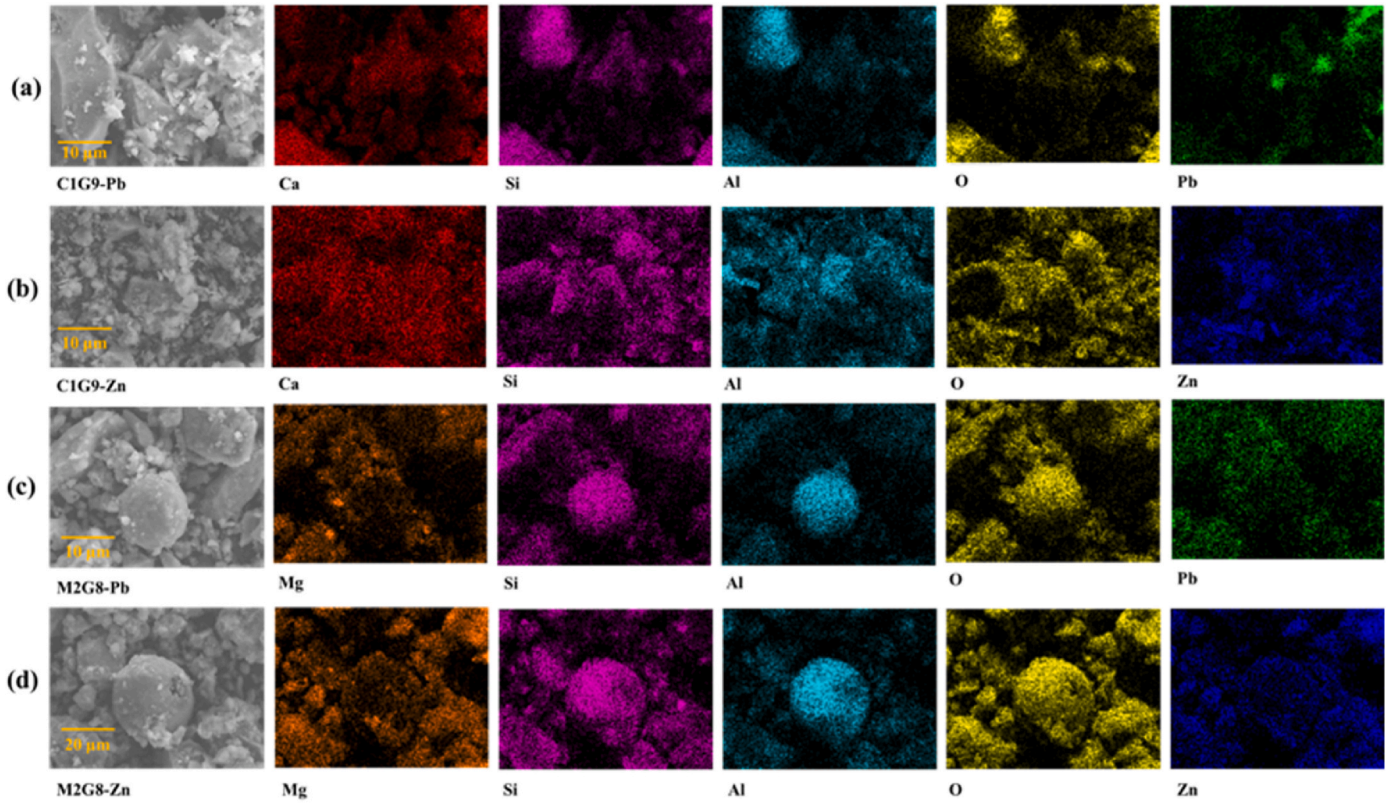

Fig. 7. SEM and elemental mapping of S/S pastes.

the TGA results. New peaks of PbO and Pb_2SiO_4 ($2PbO{\cdot}SiO_2$) appeared in the C1G9-Pb pattern, indicating that the leachable Pb ions could be precipitated in the alkaline environment as an oxide form. It was reported that Pb_2SiO_4 could wrap or cover the surface of the cementitious powder and halt the reaction process (Wang et al., 2018). As for the C1G9-Zn sample, new peaks of $Ca(Zn(OH)_3)_2{\cdot}2H_2O$ and ZnO could be identified. Garg and White (2017) reported that the precipitation of $Ca(Zn(OH)_3)_2{\cdot}2H_2O$ would terminate the reaction process by covering the surface of GGBS powder, disrupting the nucleation and growth of C–S–H gel. As for the MgO-GGBS system (M2G8) with PTEs (Fig. 6b), a signal of $Mg(OH)_2$ could be observed in the Pb and Zn incorporated pastes, which were negligible in the pure M2G8 system. The accumulation of $Mg(OH)_2$ could be attributed to the suppression from $Mg(OH)_2$ to M-S-H gel by PTEs. No apparent peaks of metal-containing crystal compounds existed in the M2G8-Pb or M2G8-Zn samples. Therefore, leachable Pb or Zn ions might be stabilized by encapsulation in hydration products, such as $Mg(OH)_2$ (Wang and Wang, 2022).

The SEM-EDX mapping showed that PTEs would be enriched in a certain part of precipitation in the CaO-GGBS system, whereas PTEs were uniformly stabilized by abundant reaction products in the MgO-GGBS system. As shown in Fig. 7a&b, the blocky structure could be found in the C1G9-Pb pastes, whereas abundant granular structure, possibly representing the unreacted raw materials, was observed in the C1G9-Zn pastes. This may reflect that Zn had a relatively high inhibitory effect on the reaction of the CaO-GGBS system. From the elemental mapping, Pb seemed to overlap with Si and O, suggesting the existence of $2PbO{\cdot}SiO_2$ and PbO. The Zn was uniformly distributed in the C1G9-Zn pastes overlapping with O and Ca, i.e., in line with the existence of $Ca(Zn(OH)_3)_2{\cdot}2H_2O$ as identified by XRD results. As for the M2G8 systems, a polymerized structure could be observed in both pastes, indicating the existence of abundant hydration products with a high polymerization. Moreover, the presence of Pb or Zn was positively correlated with Mg, implying that Pb or Zn was immobilized by hydration products such as $Mg(OH)_2$ and M-S-H.

The TCLP leachability results showed that MgO-GGBS systems had relatively higher immobilization efficiencies for PTEs compared to CaO-GGBS systems. As shown in Fig. 8a, the Pb leaching concentration of C1G9-Pb (29.2 mg/L) was 14 times higher than that of M2G8-Pb (2.1 mg/L); the Zn leaching concentration of C1G9-Zn (10.2 mg/L) was even over three orders of magnitude higher than that of M2G8-Zn (0.002 mg/L). These results illustrated that the M2G8 binder provided much higher immobilization efficiency for Pb and Zn than the C1G9 binder. The pH values in the TCLP leachate of M2G8-Pb/Zn systems were at approximately 9.5, whereas the TCLP pH values were 10.5 for C1G9-Pb and 8.1 for C1G9-Zn, which were close to the most stable pH for Pb (10.2) and Zn (9.6) (Paria and Yuet, 2006). Therefore, the pH value was not the major factor resulting in such dramatic differences in the PTEs leachabilities. Based on various analytical results, the favorable reaction process and abundant reaction products in MgO-GGBS systems could be the major reason contributing to the high PTEs immobilization efficiency.

Compressive strength of the 28-day cured samples also confirmed the advantages of the MgO-GGBS system for strength development. From Fig. 8b, the compressive strength of C1G9-Pb (0.38 MPa) and C1G9-Zn (0.30 MPa) was lower than 1 MPa, which was probably because 10 wt% $Pb(NO_3)_2$ or $Zn(NO_3)_2$ suppressed the formation of C–S–H gel in CaO-GGBS systems. By comparison, the compressive strength of M2G8-Pb and M2G8-Zn reached 3.46 MPa and 1.26 MPa, respectively, which originated from the abundant $Mg(OH)_2$ gel evidenced by TGA results (Fig. 5d).

In summary, the formation of $Ca(Zn(OH)_3)_2{\cdot}2H_2O$ or $2PbO{\cdot}SiO_2$ in the CaO-GGBS system retarded the hydration process, resulting in an insufficient immobilization efficiency and low compressive strength. On the contrary, the MgO-GGBS system showed a high compatibility with PTEs, allowing for a good and reliable S/S performance.

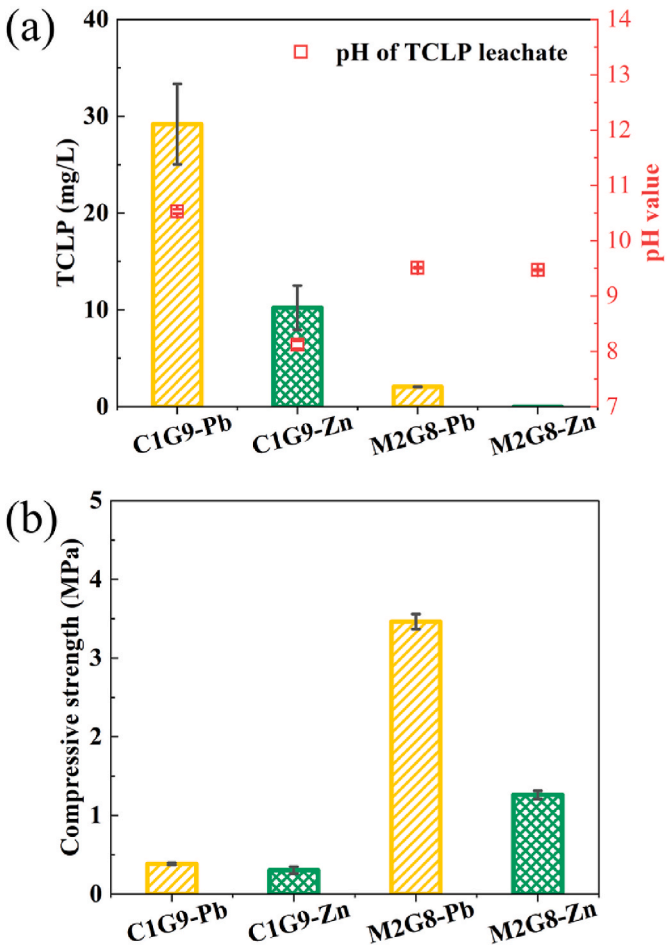

Fig. 8. TCLP leachability and compressive strength of 28-day Pb- or Zn-incorporated pastes.

3.4. CaO-/MgO-GGBS binders for S/S of MSWI FA

Practical S/S experiments further demonstrated that the MgO-GGBS binder showed a satisfying S/S performance for the MSWI FA treatment. The TCLP leachabilities of Pb and Zn from raw MSWI FA were 6.89 mg/L and 49.3 mg/L, respectively (Table S1). From Fig. 9a, with the increase of MSWI FA dosage from 50 to 90%, the TCLP leachability of Pb rose from 0.06 to 1.05 mg/L in the C1G9 system and from 0.04 to 0.48 mg/L in the M2G8 system. The Pb immobilization efficiencies of C1G9 and M2G8 were all over 97.8% and 99.0% (at a 90 wt% MSWI FA dosage), respectively. The Pb leachabilities from all the M2G8 systems were lower than those from all the C1G9 systems, which followed the trend observed in the pure metal salt incorporated pastes (Fig. 8a). As the Pb leachabilities of the pastes with 90 wt% MSWI FA exceeded the national standard limits (0.25 mg/L) (GB16889, 2008), the mixtures with 70 wt% MSWI FA were suggested to fulfil the criterion. Regarding Zn immobilization, the M2G8-based binder also performed better than the C1G9-based binder at various MSWI FA dosages, which confirmed the findings in Fig. 8a. The Zn immobilization efficiencies of C1G9 and M2G8 binders were all over 99.5% and 99.7% (at a 90 wt% dosage), respectively. Considering the loose limit of Zn leachability (100 mg/L), all the S/S blocks fulfil the requirement of the national standard (GB16889, 2008).

Compressive strength of all the MSWI FA S/S blocks is presented in Fig. 9c. Pure C1G9 and M2G8 samples had a compressive strength of 30.9 MPa and 27.3 MPa, respectively. After 50 wt% MSWI incorporation, C1G9F5 and M2G8F5 showed a comparable compressive strength, ca. 23 MPa, which was slightly weaker than the reference blocks. When

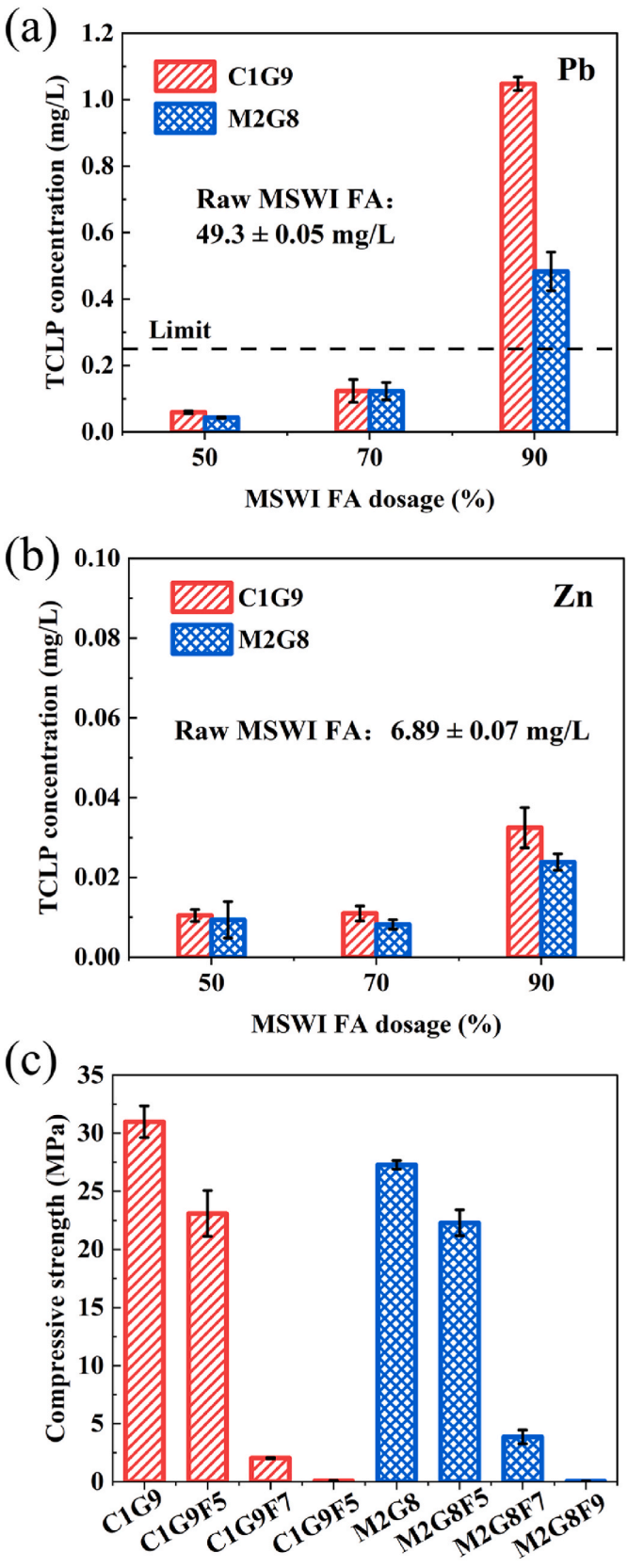

Fig. 9. TCLP leachability and compressive strength of MSWI FA S/S blocks.

the MSWI FA dosage increased to 70 wt%, the strength of C1G9F7 and M2G8F7 samples significantly decreased. Interestingly, the strength of the M2G8F7 sample (3.9 MPa) surpassed that of C1G9F7 sample (2.0 MPa), which showed an opposite trend in comparison with the pure blocks. These results showed that the MgO-GGBS system had better compatibility with leachable Zn or Pb from MSWI FA, which confirmed the trend in Fig. 8b. As the incorporation ratio increased to 90%, the strength of both S/S systems was inadequate. Therefore, the C1G9F5 and M2G8F5 mixtures with 50 wt% MSWI FA were suggested for producing high-performance S/S blocks, whereas M2G8F7 with 70 wt% MSWI FA were economical and sufficient for producing low-grade construction materials with acceptable PTEs leachability (immobilization efficiency of 99.8% for Zn and 99.7% for Pb) and compressive strength. It should be noted that such MSWI FA-incorporated blocks could not offer satisfactory compressive strength requirements of construction materials for structure use (>30 MPa), which limits the application field of MSWI FA-derived S/S blocks. Moreover, the durability of such S/S blocks under environmental attacks should be further evaluated in view of both mechanical strengths and PTEs leachabilities.

4. Conclusions

This study designed low-carbon CaO and MgO-activated GGBS binders for S/S of PTEs-rich MSWI FA. Compared to the CaO-GGBS binder, the MgO-GGBS binder had better compatibility with PTEs. Multiscale characterization revealed that the incorporation of Zn or Pb in the CaO-GGBS system form $Ca(Zn(OH)_3)_2{\cdot}2H_2O$ or $2PbO{\cdot}SiO_2$ precipitates, which inhibited the reaction of CaO-GGBS and resulted in insufficient reaction products (e.g., $Ca(OH)_2$ and C–S–H gel). However, Zn or Pb did not hinder the transformation from MgO to $Mg(OH)_2$ in the MgO-GGBS system. The abundant reaction products (e.g., $Mg(OH)_2$ and M-S-H gel) in the MgO-GGBS system allowed for high PTEs immobilization efficiencies and compressive strengths. Practical S/S experiments demonstrated that MgO-GGBS could serve as a high-efficiency binder for S/S of MSWI FA and the derived pastes with 70 wt% MSWI FA demonstrated an outstanding PTEs leachability and compressive strength. Overall, this study provides mechanistic insights into the interactions between CaO-/MgO-GGBS binders and PTEs in MSWI FA and innovates a promising MgO-GGBS binder for low-carbon S/S of hazardous wastes.

Credit author statement

Chen Sun: Conceptualization, Methodology, Data curation, Investigation, Writing - Original draft preparation; **Weizhe Ge:** Methodology, Data curation, Investigation; **Yuying Zhang:** Methodology, Investigation, Writing - Review & Editing; **Lei Wang:** Conceptualization, Methodology, Investigation, Supervision, Validation, Project administration, Resources, Funding acquisition, Writing - Review & Editing; **Yan Xia**: Methodology, Investigation, Writing - Review & Editing; **Xiaoqing Lin:** Validation, Writing - Review & Editing; **Qunxing Huang:** Resource; **Shengyong Lu:** Resources; **Daniel C.W. Tsang:** Validation, Resources, Writing - Review & Editing; **Jianhua Yan:** Funding acquisition, Resources, Writing - Review & Editing.

Declaration of competing interest

The authors declare that they have no known competing financial interests or personal relationships that could have appeared to influence the work reported in this paper.

Data availability

Data will be made available on request.

Acknowledgements

The authors gratefully acknowledge the financial support from the National Natural Science Foundation of China (No. 52206174) and the Open Project of State Key Laboratory of Clean Energy Utilization, Zhejiang University (ZJUCEU2022001) for this study.

Appendix A. Supplementary data

Supplementary data to this article can be found online at https://doi.org/10.1016/j.jenvman.2023.117938.

References

Abdalqader, A.F., Jin, F., Al-Tabbaa, A., 2016. Development of greener alkali-activated cement: utilisation of sodium carbonate for activating slag and fly ash mixtures. J. Clean. Prod. 113, 66–75.
BS EN 12390-3, 2009. Testing Hardened Concrete Compressive Strength of Test Specimens. British Standards Institution, London, UK.
Chen, Z., Ye, H., 2022. The role of CaO and MgO incorporation in chloride resistance of sodium carbonate-activated slag. Cem. Concr. Compos. 132, 104625.
Chen, L., Zhang, Y., Wang, L., Ruan, S., Chen, J., Li, H., et al., 2022. Biochar-augmented carbon-negative concrete. Chem. Eng. J. 431, 133946.
Fan, C., Wang, B., Ai, H., Liu, Z., 2022. A comparative study on characteristics and leaching toxicity of fluidized bed and grate furnace MSWI fly ash. J. Environ. Manag. 305, 114345.
Funari, V., Braga, R., Bokhari, S.N.H., Dinelli, E., Meisel, T., 2015. Solid residues from Italian municipal solid waste incinerators: a source for “critical” raw materials. Waste Manage. (Tucson, Ariz.) 45, 206–216.
Garg, N., White, C.E., 2017. Mechanism of zinc oxide retardation in alkali-activated materials: an in situ X-ray pair distribution function investigation. J. Mater. Chem. 5, 11794–11804.
GB 34330, Identification standards for solid wastes-general rules. Ministry of Ecology and Environment, China, 2017.
GB 16889, 2008. Standard for pollution control on the landfill site of municipal solid waste. Ministry of Environmental Protection, China.
GB 18485, 2014. Standard for pollution control on the municipal solid waste incineration. Ministry of Ecology and Environment, China.
Guo, B., Tan, Y., Wang, L., Chen, L., Wu, Z., Sasaki, K., et al., 2021. High-efficiency and low-carbon remediation of zinc contaminated sludge by magnesium oxysulfate cement. J. Hazard Mater. 408, 124486.
Haha, M.B., Lothenbach, B., Le Saout, G., Winnefeld, F., 2011. Influence of slag chemistry on the hydration of alkali-activated blast-furnace slag — Part I: effect of MgO. Cement Concr. Res. 41, 955–963.
Haha, M.B., Lothenbach, B., Le Saout, G., Winnefeld, F., 2012. Influence of slag chemistry on the hydration of alkali-activated blast-furnace slag-Part II: effect of Al_2O_3. Cement Concr. Res. 42, 74–83.
Hay, R., Celik, K., 2020. Accelerated carbonation of reactive magnesium oxide cement (RMC)-based composite with supercritical carbon dioxide ($scCO_2$). J. Clean. Prod. 248, 119282.
Jin, F., Al-Tabbaa, A., 2013. Thermogravimetric study on the hydration of reactive magnesia and silica mixture at room temperature. Thermochim. Acta 566, 162–168.
Lan, T., Meng, Y., Ju, T., Chen, Z., Du, Y., Deng, Y., et al., 2022. Synthesis and application of geopolymers from municipal waste incineration fly ash (MSWI FA) as raw ingredient - a review. Resour. Conserv. Recycl. 182, 106308.
Li, W., Ni, P., Yi, Y., 2019. Comparison of reactive magnesia, quick lime, and ordinary Portland cement for stabilization/solidification of heavy metal-contaminated soils. Sci. Total Environ. 671, 741–753.
Li, Z., Lu, D., Gao, X., 2020. Analysis of correlation between hydration heat release and compressive strength for blended cement pastes. Construct. Build. Mater. 260, 120436.
Liew, R.K., Chai, C., Yek, P.N.Y., Phang, X.Y., Chong, M.Y., Nam, W.L., et al., 2019. Innovative production of highly porous carbon for industrial effluent remediation via microwave vacuum pyrolysis plus sodium-potassium hydroxide mixture activation. J. Clean. Prod. 208, 1436–1445.
Liu, J., Jin, H., Gu, C., Yang, Y., 2019. Effects of zinc oxide nanoparticles on early-age hydration and the mechanical properties of cement paste. Construct. Build. Mater. 217, 352–362.
Ma, W., Chen, D., Pan, M., Gu, T., Zhong, L., Chen, G., et al., 2019. Performance of chemical chelating agent stabilization and cement solidification on heavy metals in MSWI fly ash: a comparative study. J. Environ. Manag. 247, 169–177.
Martini, F., Tonelli, M., Geppi, M., Ridi, F., Borsacchi, S., Calucci, L., 2017. Hydration of MgO/SiO_2 and Portland cement mixtures: a structural investigation of the hydrated phases by means of X-ray diffraction and solid state NMR spectroscopy. Cement Concr. Res. 102, 60–67.
NBSC, 2020. China Statistical Yearbook of 2020 Chinese. National Bureau of Statistics of China, Beijing China.
Paria, S., Yuet, P.K., 2006. Solidification–stabilization of organic and inorganic contaminants using portland cement: a literature review. Environ. Rev. 14, 217–255.
Quina, M.J., Bordado, J.C., Quinta-Ferreira, R.M., 2008. Treatment and use of air pollution control residues from MSW incineration: an overview. Waste Manage. (Tucson, Ariz.) 28, 2097–2121.

Ren, Z., Wang, L., Wang, H., Liu, S., Liu, M., 2023. Solidification/stabilization of lead-contaminated soils by phosphogypsum slag-based cementitious materials. Sci. Total Environ. 857, 159552.
Rheinheimer, V., Unluer, C., Liu, J., Ruan, S., Pan, J., Monteiro, P.J.M., 2017. XPS study on the stability and transformation of hydrate and carbonate phases within MgO systems. Materials 10, 75.
Trauchessec, R., Mechling, J.M., Lecomte, A., Roux, A., Le Rolland, B., 2015. Hydration of ordinary Portland cement and calcium sulfoaluminate cement blends. Cement Concr. Compos. 56, 106–114.
US EPA 1311, 1992. Toxicity Characteristic Leaching Procedure. US Environ. Prot. Agency, Washington, DC, USA.
Walkley, B., Provis, J.L., 2019. Solid-state nuclear magnetic resonance spectroscopy of cements. Mater. Today Adv. 1, 100007.
Walling, S.A., Provis, J.L., 2016. Magnesia-based cements: a journey of 150 years, and cements for the future? Chem. Rev. 116, 4170–4204.
Wang, B., Fan, C., 2020. Hydration behavior and immobilization mechanism of $MgO–SiO_2–H_2O$ cementitious system blended with MSWI fly ash. Chemosphere 250, 126269.
Wang, D., Wang, Q., 2022. Clarifying and quantifying the immobilization capacity of cement pastes on heavy metals. Cement Concr. Res. 161, 106945.
Wang, Y.S., Dai, J.G., Wang, L., Tsang, D.C.W., Poon, C.S., 2018. Influence of lead on stabilization/solidification by ordinary Portland cement and magnesium phosphate cement. Chemosphere 190, 90–96.
Wang, L., Geddes, D.A., Walkley, B., Provis, J.L., Mechtcherine, V., Tsang, D.C.W., 2020. The role of zinc in metakaolin-based geopolymers. Cement Concr. Res. 136, 106194.
Wang, L., Zhang, Y., Chen, L., Guo, B., Tan, Y., Sasaki, K., et al., 2022. Designing novel magnesium oxysulfate cement for stabilization/solidification of municipal solid waste incineration fly ash. J. Hazard Mater. 423, 127025.
Whittaker, M., Zajac, M., Ben Haha, M., Bullerjahn, F., Black, L., 2014. The role of the alumina content of slag, plus the presence of additional sulfate on the hydration and microstructure of Portland cement-slag blends. Cement Concr. Res. 66, 91–101.
Xia, Y., Liu, M., Zhao, Y., Chi, X., Guo, J., Du, D., et al., 2023a. Hydration mechanism and phase assemblage of blended cement with iron-rich sewage sludge ash. J. Build. Eng. 63, 105579.
Xia, Y., Liu, M., Zhao, Y., Chi, X., Lu, Z., Tang, K., et al., 2023b. Utilization of sewage sludge ash in ultra-high performance concrete (UHPC): microstructure and life-cycle assessment. J. Environ. Manag. 326, 116690.
Yek, P.N.Y., Peng, W., Wong, C.C., Liew, R.K., Ho, Y.L., Wan Mahari, W.A., et al., 2020. Engineered biochar via microwave CO_2 and steam pyrolysis to treat carcinogenic Congo red dye. J. Hazard Mater. 395, 122636.
Zhang, W.L., Zhao, L.Y., McCabe, B.A., Chen, Y.H., Morrison, L., 2020. Dredged marine sediments stabilized/solidified with cement and GGBS: factors affecting mechanical behaviour and leachability. Sci. Total Environ. 733, 138551.
Zhang, Y., Wan, Z., Wang, L., Guo, B., Ma, B., Chen, L., et al., 2022. Designing magnesium phosphate cement for stabilization/solidification of Zn-rich electroplating sludge. Environ. Sci. Technol. 56, 9398–9407.
Zhou, Y., Cai, G., Cheeseman, C., Li, J., Poon, C.S., 2022. Sewage sludge ash-incorporated stabilisation/solidification for recycling and remediation of marine sediments. J. Environ. Manag. 301, 113877.